
Multi-modal Self-Supervision from Generalized Data Transformations

Mandela Patrick^{1,2*} Yuki M. Asano^{2*} Polina Kuznetsova¹ Ruth Fong²
João F. Henriques² Geoffrey Zweig¹ Andrea Vedaldi^{1,2}

¹ Facebook AI Research
mandelapatrik@fb.com

² Visual Geometry Group, University of Oxford
yuki@robots.ox.ac.uk

Abstract

The recent success of self-supervised learning can be largely attributed to content-preserving transformations, which can be used to easily induce invariances. While transformations generate positive sample pairs in contrastive loss training, most recent work focuses on developing new objective formulations, and pays relatively little attention to the transformations themselves. In this paper, we introduce the framework of Generalized Data Transformations to (1) reduce several recent self-supervised learning objectives to a single formulation for ease of comparison, analysis, and extension, (2) allow a choice between being invariant or distinctive to data transformations, obtaining different supervisory signals, and (3) derive the conditions that combinations of transformations must obey in order to lead to well-posed learning objectives. This framework allows both invariance and distinctiveness to be injected into representations simultaneously, and lets us systematically explore novel contrastive objectives. We apply it to study multi-modal self-supervision for audio-visual representation learning from unlabelled videos, improving the state-of-the-art by a large margin, and even surpassing supervised pretraining. We demonstrate results on a variety of downstream video and audio classification and retrieval tasks, on datasets such as HMDB-51, UCF-101, DCASE2014, ESC-50 and VGG-Sound. In particular, we achieve new state-of-the-art accuracies of 72.8% on HMDB-51 and 95.2% on UCF-101.

1 Introduction

Self-supervised pretraining of image representations is maturing rapidly, and is now competitive with pretraining methods that use manual supervision. Previous work has explored different approaches for pretraining, such as various pretext tasks [25, 33, 74, 81, 110] and clustering [8, 14, 34]. However, many recent approaches, including PIRL [69], MoCo [41] and SimCLR [98], all use noise contrastive learning. The key idea is to constrain the learned representation to be *invariant* to nuisance transformations that leave the meaning of the data unchanged (e.g. cropping an image) and *distinctive* to changes that are likely to alter its meaning (e.g. replacing an image with another chosen at random). This is cast as minimizing the so called *noise contrastive loss* [36, 37], leading to robust and effective learning.

Most of the art in designing good contrastive formulations is in the choice of the transformations. In computer vision, most formulations seek invariance to *photo-geometric* data transformations, in the form of random 2D image distortions such as scale changes, crops, or contrast changes. While these

*Joint first authors

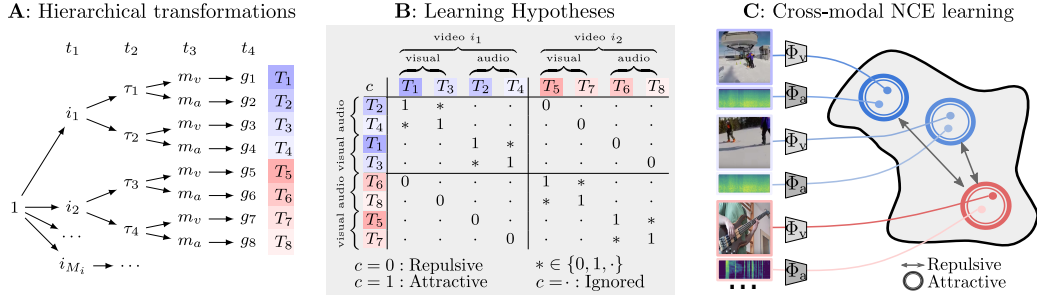


Fig. 1: Schematic overview of our framework. **A:** Hierarchical sampling process of generalized transformations $T = t_M \circ \dots \circ t_1$ for the multi-modal training study case. **B:** With generalized data transformations (GDT), the network learns a meaningful embedding via learning desirable invariances and distinctiveness to transformations (realigned here for clarity) across modalities and time. The embedding is learned via noise contrastive estimation against clips of other source videos. **C:** Subset of the $c(T, T')$ contrast matrix which shows which pairs are repelling (0) and attracting (1) (see text for details). Illustrational videos taken from [1].

only approximate real nuisance factors such as a viewpoint change, object deformations or intra-class variations, the key advantage is that they can be trivially implemented. For distinctiveness, these formulations seek to discriminate different image samples, assuming that the probability that two random images have the same ‘meaning’ is very low.

Compared to images, videos allow for pretraining methods exploiting time- and multi-modality based transformations [6, 55, 112]. An example is cross-modal supervision [6, 78], where one learns to match the visual and audio components extracted from the same video. The latter is an excellent proxy for abstraction as it encourages the representation to learn objects with a characteristic appearance and sound. Others [20, 55, 77] have proposed to look at the temporal correlation between the audio and visual streams, learning to tell whether they are in sync or not. Notably, these methods are usually *not* formulated in a noise contrastive manner. Overall, we can paint a complex picture, with different methods learning from a different combination of cues and learning schemes.

In this paper, we introduce the method of *generalized data transformation (GDT)* which clarifies, unifies and improves these different methodological approaches. A GDT absorbs in one object effects such as data sampling, choice of a modality, time shift, and photo-geometric augmentation. Given this, one can reduce most existing self-supervised learning schemes to (1) choosing how GDTs are sampled in a batch and (2) which GDT pairs are contrasted positively, negatively, or are ignored. This concept is exemplified in Figure 1 in a typical instantiation for audio-visual learning. A set of GDTs are constructed hierarchically, starting from sampling videos from a dataset down to splitting modalities and applying augmentations (A). Then, different pairs of transformations are contrasted with a positive (attractive) or negative (repulsive) effect (B). This learns corresponding invariances or distinctiveness in the representation (C).

The importance of our reduction is that it extends to cues that have been so far given only in a non-contrastive manner, and allows for novel combinations previously unexplored, such as distinctiveness to time shift and time reversal across modalities, yielding state-of-the-art feature representations. We also derive formal conditions to tell which combinations are valid. Furthermore, most contrastive formulations are concerned with the choice of invariances, fixing distinctiveness to the discrimination of different samples. The GDT framework shows that both design choices can be changed, leading to better results.

In short, a key benefit of GDTs is that they allow to systematically explore and test novel *hypotheses* on which invariances and distinctivenesses are most beneficial for pretraining data representations. Because of this added flexibility, we can *improve* the performance of existing approaches. To demonstrate this, we apply our framework to multi-modal (video) data, as it offers a rich space of combinations to search. Using our framework, we explore the space of such combinations and determine which ones are optimal for downstream performance. With this, we are able to set the new state of the art in audio-visual representation learning, with both small and large video pretraining datasets on a variety of visual and audio downstream tasks. In particular, we achieve 95.2% and 72.8% on the standardized UCF-101 and HMDB-51 action recognition benchmarks.

2 Related work

Early unsupervised representation learning. Learning representations from unlabelled data has been an active area of computer vision research for decades. Early works such as auto-encoders [43], deep belief networks [44], shift-invariant decoders [86], sparse coding algorithms [59] and stacked ISAs [58] learned image and video representations by reconstructing inputs. Recently, however, a number of works have instead focused on self-supervised learning approaches to learn representations by developing *pretext tasks* to encourage networks to learn semantics from the free supervision signals available in images and videos.

Self-supervised learning from images and videos. A variety of pretext tasks have been proposed to learn representations from unlabelled **images**. Some tasks leverage the spatial context in images [24, 74] to train CNNs, while others create pseudo classification labels via artificial rotations [33], or clustering features [8, 14, 15, 34]. Colorization [110, 111], inpainting [81], solving jigsaw puzzles [75], as well as the contrastive methods detailed below, have been proposed for self-supervised image representation learning. Some of the tasks that use the space dimension of images have been extended to the space-time dimensions of **videos** by crafting equivalent tasks. These include jigsaw puzzles [53], and predicting rotations [49] or future frames [38]. Other tasks leverage the temporal dimension of videos to learn representations by predicting shuffled frames [70], the direction of time [105], motion [104], clip and sequence order [60, 109], and playback speed [11, 19, 26]. These pretext-tasks can be framed as GDTs.

Multi-modal learning. Videos, unlike images, are a rich source of a variety of modalities such as speech, audio, and optical flow, and their correlation can be used as a supervisory signal. This idea has been present as early as 1993 [22]. Only recently, however, has multi-modal learning been used to successfully learn effective representations by leveraging the natural correspondence [5, 6, 9, 71, 78] and synchronization [20, 55, 77] between the audio and visual streams. A number of recent papers have leveraged speech as a weak supervisory signal to train video representations [62, 68, 72, 96, 97]. Other works incorporate optical flow and other modalities [64, 83, 98, 114] to learn representations. Furthermore, multi-modal learning has been used for several applications such as lip reading [4, 20, 21], audio-visual source separation and localization [3, 7, 28, 29, 39, 77, 87, 91, 113, 114], speech recognition [2, 73, 84], efficient inference [30, 56], egocentric action recognition [51] and navigation [16]. The space for **transformations** is much richer in video than images due to the audio and visual streams. Crucially, videos have high frame rates, which allows for a large combinatorial space of cropping in time *and* space [5, 6, 38, 55, 92, 100]. Videos also contain useful multi-modal signals such as audio-visual synchronization [6, 20, 55, 77].

Noise Contrastive Loss. Noise contrastive losses [36, 37] measure the similarity between sample pairs in a representational space and are at the core of several recent works on unsupervised feature learning. It has been shown to yield good performance for learning image [18, 41, 42, 45, 61, 69, 76, 98, 99, 106] and video [38, 62, 68, 71, 93, 96] representations, and circumvents the need to explicitly specify what information needs to be discarded via a designed task. We leverage the noise contrastive loss as a learning framework to encourage the network to learn desired invariance and distinctiveness to data transformations.

The GDT framework can be used to combine and extend many of these cues, contrastive or not, in a single noise contrastive formulation.

3 Method

A *data representation* is a function $f : \mathcal{X} \rightarrow \mathbb{R}^D$ mapping data points x to vectors $f(x)$. Representations are useful because they help to solve data analysis tasks that are of interest in applications, such as classifying images. Based on the nature of the data and the task, we often know a priori some of the invariances that the representation should possess. We can capture those by means of the *contrast* function² $c(x_1, x_2) = \delta_{f(x_1)=f(x_2)}$, where $c(x_1, x_2) = 1$ means that f is *invariant* to replacing x_1 with x_2 , while $c(x_1, x_2) = 0$ means that f is *distinctive* for this change. Any partial knowledge of the contrast c can be used as a cue to learn f . However, we cannot choose c in an arbitrary manner; in order for c to define a function f consistently, the expression $c(x_1, x_2) = 1$ must

²We use the symbol δ to denote the Kronecker delta.

be an *equivalence relation* on \mathcal{X} , i.e. be reflexive $c(x, x) = 1$, symmetric $c(x_1, x_2) = c(x_2, x_1)$ and transitive $c(x_1, x_2) = c(x_2, x_3) = 1 \Rightarrow c(x_1, x_3) = 1$. This is justified in Appendix A.1.

Next, we introduce *generalized data transformations* by considering two examples of contrastive learning formulations. The first example is analogous to ‘standard’ methods such as MoCo [41] and SimCLR [18], whereas the second tackles multi-modal data.

Standard contrastive formulation. We wish to learn the representation f to match a known contrast c . In order to do so, we require samples x_1 and x_2 forming both invariant $c(x_1, x_2) = 1$ and distinctive $c(x_1, x_2) = 0$ pairs. Positive pairs can be generated by sampling x_1 and then by setting $x_2 = g(x_1)$ as a random transformation of the first sample, where $g \in \mathcal{G}$ is called a data *augmentation*. Negative pairs are obtained by sampling x_1 and x_2 independently.

It is convenient to express these concepts via transformations only. To this end, let $D = (x_1, \dots, x_N) \in \mathcal{X}^N$ be the collection of N unlabelled i.i.d. training data samples. A *Generalized Data Transformation* (GDT) $T : \mathcal{X}^N \rightarrow \mathcal{Z}$ is a mapping that acts on the set of training samples D to produce a new sample $z = TD$. Note that the GDT is applied to the entire training set, so that sampling itself can be seen as a transformation. In the simplest case, the GDT output $TD \in \mathcal{Z} = \mathcal{X}$ is obtained by (i) extracting the i -th data sample and by (ii) applying an augmentation $g : \mathcal{X} \rightarrow \mathcal{X}$ to it. Formally, the action of $T = (i, g)$ is $TD = g(x_i)$.

In our ‘standard’ formulation, learning seeks for a function f that is *distinctive* for the choice of sample but *invariant* to its augmentation, which is expressed by the contrast $c(T, T') = c((i, g), (i', g')) = \delta_{i=i'}$. Note that, differently from the previous section, we have now defined c on transformations T rather than on samples x . In Appendix A.1, we show that this is acceptable provided that $c(T, T') = 1$ is also reflexive, symmetric, and transitive.

Next, we consider a batch $\mathcal{T} = \{T_1, \dots, T_K\}$ of K GDTs and optimize the so-called *noise-contrastive loss* [18, 36, 76, 98, 106] over it:

$$\mathcal{L}(f; \mathcal{T}) = - \sum_{T, T' \in \mathcal{T}} c(T, T') w(T, T') \log \left(\frac{\exp \langle f(TD), f(T'D) \rangle / \rho}{\sum_{T'' \in \mathcal{T}} w(T, T'') \exp \langle f(TD), f(T''D) \rangle / \rho} \right), \quad (1)$$

where the scalar ρ is a temperature parameter. The weights $w(T, T')$ are set to $\delta_{T \neq T'}$ in order to discount contrasting identical transformations, which would result in a weak learning signal.

We can think of eq. (1) as a softmax cross-entropy loss for a classification problem where the classes are the equivalence classes \mathcal{T}/c of transformations. Minimizing eq. (1) pulls together vectors $f(TD)$ and $f(T'D)$ if $c(T, T') = 1$ and pushes them apart if $c(T, T') = 0$. The effect is similar to a margin loss, but with a better handling of hard negatives [18, 52, 98].

Multi-modal contrastive formulation. Several papers have suggested to use the correlation between modalities to learn representations for multi-modal data [6, 9, 55, 78, 105]. While this is usually not done in a noise-contrastive manner, here we show that the formulation above extends immediately to this case. For this, let x_1 and x_2 be two different modalities of the same underlying data sample x . In order to encode this with a GDT, consider *modality projection* transformations $m \in \mathcal{M}$. For example, a video $x = (v, a)$ has a visual component v and an audio component a and $\mathcal{M} = \{m_a, m_v\}$ contains projections $m_v(x) = v$ and $m_a(x) = a$ on the two components. With this, we can modify the ‘standard’ formulation given above to use GDTs $T = (i, m)$ with action $TD = m(x_i)$. Minimizing eq. (1) now learns a representation f which is distinctive for the choice of input video, but invariant to the choice of modality. For this, as f must accept either a visual or audio signal as input, we consider a pair of representations $f = (f_v, f_a)$, one for each modality.³

3.1 Combining multiple invariance and distinctiveness cues

We have suggested above that GDTs can capture standard contrastive and other self-supervised learning formulations. In this section, we show how the framework can in fact accommodate complex combinations of transformations, capturing invariance to some and distinctiveness to others, thus leading to new formulations. In order to instantiate eq. (1), in fact, we only require: (1) the contrast $c(T, T')$ and (2) a way of sampling transformations in the batch.

³Formally, we set videos $\mathcal{X} = \mathcal{X}_v \times \mathcal{X}_a$ to be visual-audio pairs $x = (v, a)$, $\mathcal{Z} = \mathcal{X}_v \oplus \mathcal{X}_a$ to be the direct sum of these two domains, $m : \mathcal{X} \rightarrow \mathcal{Z}$ to be a projection function extracting either component, and $f_v : \mathcal{X}_v \rightarrow \mathbb{R}^D$ and $f_a : \mathcal{X}_a \rightarrow \mathbb{R}^D$ a corresponding pair of learnable representation functions.

Differently from common learning formulations that work with independent samples, in contrastive learning, one *must* ensure that the batch contains transformations that can be meaningfully contrasted, forming a mix of invariant and distinctive pairs. This means that transformations cannot be sampled independently. Instead, we propose the following *hierarchical* sampling scheme. Each generalized transformation $T = t_M \circ \dots \circ t_1$ is constructed as a sequence of M transformations t_m . First, we sample K_1 instances of transformation t_1 ; then, for each sample t_1 , we sample K_2 instances of transformation t_2 and so on, obtaining a total of $K = \prod_{m=1}^M K_m$ different transformations T for the batch. Given two generalized transformations $T = t_M \circ \dots \circ t_1$ and $T' = t'_M \circ \dots \circ t'_1$ sampled in this manner, we must also define $c(T, T')$. For individual transformations, we set

$$c(t_m, t'_m) = \begin{cases} 1, & \text{if we hypothesize invariance,} \\ \delta_{t_m=t'_m}, & \text{if we hypothesize distinctiveness.} \end{cases} \quad (2)$$

and define $c(T, T') = \prod_{m=1}^M c(t_m, t'_m)$. In Appendix A.1, we justify this choice by showing that, if the individual $c(t_m, t'_m)$ are reflexive, symmetric and transitive, so is $c(T, T')$. Intuitively, this sampling scheme is a simple way of controlling how transformations in a batch differ, and thus which properties can be learned by contrasting them.

We show in Appendix A.2 that this framework can be used to express various self-supervised learning cues that have been proposed in the literature, and show an example for audio-visual data next.

3.2 Exploring contrastive audio-visual self-supervision

In order to apply our framework to audio-visual data, we start by specify how transformations are sampled by using the hierarchical scheme introduced above (see also Figure 1). We consider in particular GDTs of the type $T = (i, \tau, m, g)$ combining the following transformations. The first component i **selects** a video in the dataset. We sample $K_i \gg 2$ indices/videos and assume distinctiveness, so that $c(i, i') = \delta_{i=i'}$. The second component τ contrasts different **temporal shifts**. We sample $K_\tau = 2$ different values of a delay τ uniformly at random, extracting a 1s clip $x_{i\tau}$ starting at time τ . For this contrast, we will test the distinctiveness and invariance hypotheses (see below). The third component m contrasts **modalities**, projecting the video $x_{i\tau}$ to either its visual or audio component $m(x_{i\tau})$. We assume invariance $c(m, m') = 1$ and always sample two such transformations m_v and m_a to extract both modalities, so $K_m = 2$. The fourth and final component g applies a spatial and aural **augmentation** $TD = g(m(x_{i\tau}))$, also normalizing the data. We assume invariance $c(g, g') = 1$ and pick $K_g = 1$. The transformation g comprises a pair of augmentations (g_v, g_a) , where $g_v(v)$ extracts a fixed-size tensor by resizing to a fixed resolution a random spatial crop of the input video v , and $g_a(a)$ extracts a spectrogram representation of the audio signal followed by SpecAugment [79] with frequency and time masking. These choices lead to $K = K_i K_\tau K_m K_g = 4K_i$ transformations T in the batch \mathcal{T} .

Testing invariance and distinctiveness hypotheses. The transformations given above combine cues that were partly explored in prior work, contrastive and non-contrastive. For example, [55] (not noise-contrastive) learns to detect temporal shifts. With our formulation, we can test whether distinctiveness or invariance to shifts is preferable, simply by setting $c(\tau, \tau') = 1$ or $c(\tau, \tau') = \delta_{\tau=\tau'}$ (this is illustrated in fig. 1). We can also set $w(\tau, \tau') = 0$ for $\tau \neq \tau'$ to ignore comparisons that involve different temporal shifts. We also test distinctiveness and invariance to **time reversal** [105], which has not previously been explored cross-modally, or contrastively. This is given by a transformation $r \in \mathcal{R} = \{r_0, r_1\}$, where r_0 is the identity and r_1 flips the time dimension of its input tensor. Our method can also be used to investigate any future transformations that can yield a useful signal.

Ignoring comparisons. Another degree of freedom is the choice of weighting function $w(T, T')$. Empirically, we found that cross-modal supervision is a much stronger signal than within-modality supervision, so if T and T' slice the same modality, we set $w(T, T') = 0$ (see Appendix for ablation).

Understanding combinations. Finally, one may ask what is the effect of combining several different transformations in learning the representation f . A first answer is the rule given in Sec. 3.1 to combine individual contrasts $c(t_m, t'_m)$ in a consistent manner. Because of this rule, to a first approximation, f possesses the union of the invariances and distinctiveness of the individual factors. To obtain a more accurate answer, however, one should also account for the details of the batch sampling scheme and of the choice of weighing function w . This can be done by consulting the diagrams given in fig. 1 by: (1) choosing a pair of transformations T_i and T_j , (2) checking the value

in the table (where 1 stands for invariance, 0 for distinctiveness and · for ignoring), and (3) looking up the composition of T_i and T_j in the tree to find out the sub-transformations that differ between them as the source of invariance/distinctiveness.

4 Experiments

We compare self-supervised methods on pretraining audio-visual representations. Quality is assessed based on how well the pretrained representation transfers to other (supervised) downstream tasks. We first study the model in order to determine the best learning transformations and setup. Then, we use the latter to train for longer and compare them to the state of the art.

Self-supervised pretraining. For pretraining, we consider the standard audio-visual pretraining datasets, Kinetics-400 [50] and AudioSet [31], and additionally, the recently released, VGG-Sound dataset [17]. Finally, we also explore how our algorithm scales to even larger, less-curated datasets and train on IG65M [32] as done in XDC [5].

Our method learns a pair of representations $f = (f_v, f_a)$ for visual and audio information respectively. We use R(2+1)D-18 [101] as the visual encoder f_v and ResNet [40] with 9 layers as the audio encoder f_a unless otherwise noted; both encoders produce a fixed-dimensional output (512-D) after global spatio-temporal average pooling. Both vectors are then passed through two fully-connected layers with intermediate size of 512 to produce 256-D embeddings as in [10] which are normalized by their L2-norm [106]. The embedding is used for computing the contrastive loss, while for downstream tasks, a linear layer after the global spatio-temporal average pooling is randomly initialized. Further implementation details are given in the Appendix.⁴

Downstream tasks. To assess the **visual** representation f_v , we consider standard action recognition benchmark datasets, UCF-101 [94] and HMDB-51 [57]. We test the performance of our pretrained models on the tasks of finetuning the pretrained representation, conducting few-shot learning and video action retrieval. To assess the **audio** representation f_a , we train a linear classifier on frozen features for the common ESC-50 [82] and DCASE2014 [95] benchmarks and finetune for VGG-Sound [17]. Details are given in appendix A.4.

4.1 Analysis of generalized transformations

In this section, we conduct an extensive study on each parameter of the GDT transformation studied here, $T = (i, \tau, m, g)$, and evaluate the performance by finetuning our network on the UCF-101 and HMDB-51 action recognition benchmarks, see Appendix for implementation details.

Sample distinctiveness and invariances. First, we experiment with learning representations that are distinctive to sample selection only, while being invariant to other factors. This is an important base case as it is the standard approach followed by all recent self-supervised methods [18, 41, 106].

For this, consider GDT of the type $T = (i, \tau, m, g)$ described above and set $K_i = 768$ (the largest we can fit in our setup), $K_m = 2$ and $K_g = 1$ in the example, and only pick a single time shift $K_\tau = 1$. We also set all transformation components to invariance ($c(t_m, t'_m) = 1$) except the first that does sample selection.

Table 1 ablates three types of invariance: time shift τ (this is ‘removed’ by always taking the middle 1s clip in each video), visual augmentation g_v (removed by taking a center crop) and audio augmentation g_a (removed by never masking the spectrogram using SpecAugment). Each of these invariances are necessary to learn representations that are robust to nuisance transformations in time and modality, and prevent the model from overfitting at epoch 100.

We find that time shift invariance τ , often only implicitly enforced as a type of augmentation in other works, is essential when training neural networks in a self-supervised fashion. In particular,

Table 1: Downstream action recognition results for **different invariance ablations**.

Epochs	HMDB		UCF	
	50	100	50	100
(a) Full	55.1	56.9	85.1	87.9
(b) No τ	32.8	34.8	74.0	76.2
(c) No g_v	50.7	46.7	83.2	83.2
(d) No g_a	51.5	55.6	84.8	86.5

⁴All of our training and evaluation code is provided in the submission.

we increase downstream task performance by more than 20% on HMDB-51 and 10% on UCF-101 (row (b)).

Visual augmentation, g_v , allows the network to see more views of concepts, and leads to more robust representations, seen by an increase in performance by 10.2% for HMDB-51 and 4.5% for UCF-101 compared to simply taking center crops (row (c) at epoch 100).

Furthermore, we find that adding simple audio augmentations can further increase the performance by another 1.3% for HMDB-51 and 1.4% for UCF-101 compared to not augmenting (row (d)).

Exchanging invariance for distinctiveness. Our framework allows fine-grained and expressive control of which invariance and distinctiveness are learned. To demonstrate this flexibility, we first experiment with time shift, testing whether the invariance or distinctiveness hypothesis is better for learning. To this end, we repeat the experiment above, but setting $K_\tau = 2$. This has two effects: (1) it introduces differently-shifted variants of each video in the batch, therefore emphasizing learning this transformation and (2) it allows, based on the hierarchical sampling scheme of fig. 1, to have in the batch samples of the same video but with different shifts. Even if we still learn a representation invariant to time shift as before, (1) means that more importance is given to this factor. This is why we observe a difference in performance in table 2 (row (b) vs (a)). Note, however, that the performance *drops* for invariance to this factor, indicating that excessive insensitivity may hurt performance. However, if we switch to distinctiveness instead (row (c)), the performance improves.

We additionally extend our GDT framework to test whether the invariance or distinctiveness hypothesis to our cross-modal time reversal is better for learning transferable video representations. We set $K_\tau = 1$, but add the time reversal transformation r to our GDT $T = (i, \tau, m, g, r)$ with $K_\tau = 2$, reversing both audio and video. Similarly to time shifts, we also find that the network learns more robust, transferable representations by learning distinctiveness to time reversal (row (e) vs (d)).

These findings are noteworthy, as they contradict results from the image self-supervised learning domain, where learning pretext-invariance can lead to more transferable representations [69]. This is likely due to the fact that time shift and reversal are useful signals that both require learning strong video representations to pick up on. If instead invariance is learned against these, the “free” information that we have from construction is discarded and performance degrades.

Lastly, in the last rows of table 2, we also show the results of combining two contrastive transformations via allowing the audio and video network to have two heads each, such that the backbone can learn features useful to both tasks. For example a combination (time shift and reversal distinctiveness), previously not afforded by contrastive formulations in the literature, gives us a 3% boost on the HMDB-51 dataset over our baseline of sample distinctiveness.

4.2 Comparison to the state of the art

Given our best learning setup from Sec. 4.1, we train for longer and compare our feature representations to the state of the art in common visual and aural downstream benchmarks.

Downstream visual benchmarks. For **video retrieval** we report recall at 1, 5, 20 retrieved samples for split-1 of the HMDB-51 and UCF-101 datasets in table 4 (the results for recall at 10 and 50 are provided in the Appendix). Using our model trained on Kinetics-400, we significantly beat all other self-supervised methods by a margin of over 35% for both datasets. For **few-shot classification**, as shown in table 4, we significantly beat the RotNet3D baseline on UCF-101 by more than 10% on average for each shot with our Kinetics-400 pretrained model. For **video action recognition**, we finetune our GDT pretrained network (see Appendix for details) and compare against state-of-the-art self-supervised methods on UCF-101 and HMDB-51 video classification in table 3. When constrained to pretraining on the Kinetics datasets, we find that our GDT pretrained model

Table 2: Downstream results action recognition for **different transformation hypotheses**.

	HMDB		UCF	
	50	100	50	100
(a) Sample dist.	55.1	56.9	85.1	87.9
Time shift (TS)				
(b) invariant (I)	54.8	56.1	85.8	87.7
(c) distinct (D)	<u>56.8</u>	<u>58.2</u>	<u>86.0</u>	<u>86.5</u>
Time Reversal (TR)				
(d) invariant (I)	53.2	57.2	86.6	88.1
(e) distinct (D)	<u>54.7</u>	<u>58.0</u>	<u>87.2</u>	<u>88.5</u>
(f) TS (D), TS (I)	56.8	57.4	86.7	87.4
(g) TS (D), TR (D)	56.8	60.0	86.9	87.3
(h) TS (D), TR (I)	56.0	57.5	87.0	88.2

Table 3: **State-of-the-art on video action recognition.** Self- and fully-supervisedly trained methods on UCF-101 and HMDB-51 benchmarks. We follow the standard protocol and report the average top-1 accuracy over the official splits for finetuning the whole network. Methods with †: use video titles as supervision, with *: use ASR generated text. See table A.3 for an extended version.

(a) Models pretrained on Kinetics-400.				(b) Models pretrained on other datasets.			
Method	Architecture	Top-1 Acc%		Method	Dataset	Top-1 Acc%	
		HMDB	UCF			HMDB	UCF
Supervised	R(2+1)D-18	70.4	95.0	Supervised	Kinetics-400	70.4	95.0
CPD [62] [†] *	3D-Resnet50	57.7	88.7	GDT (ours)	VGGSound (170K)	62.1	89.4
RotNet3D [49]	3D-ResNet18	33.7	62.9	XDC [5]	AudioSet (1.8M)	61.0	91.2
DPC [38]	3D-ResNet34	35.7	75.7	AVTS [55]	AudioSet (1.8M)	61.6	89.0
Multisensory [77]	3D-ResNet18	-	82.1	AVID [71]	Audioset (1.8M)	64.7	91.5
XDC [5]	R(2+1)D-18	47.1	84.2	GDT (ours)	AudioSet (1.8M)	66.1	92.5
AVSlow-Fast [107]	AVSlowFast	54.6	87.0	MIL-NCE [68]*	HowTo100M	61.0	91.3
AVTS [55]	MC3-18	56.9	85.8	ELO [83]	Youtube-2M	67.4	93.8
AVID [71]	custom R(2+1)D	60.8	87.5	XDC [5]	IG65M	67.4	94.2
GDT (ours)	R(2+1)D-18	<u>60.0</u>	89.3	GDT (ours)	IG65M	72.8	95.2

Table 4: **Retrieval and Few Shot Learning.** Retrieval accuracy in (%) via nearest neighbors at various levels of neighborhood sizes and few shot learning accuracy (%) via training a linear SVM on fixed representations.

		HMDB			UCF		
		1	5	20	1	5	20
<i>Few-shot</i>	Random [49]	3.0	3.5	4.5	2.3	4.6	6.8
	3DRot [49]	-	-	-	15.0	31.5	47.1
	GDT (ours)	13.4	15.6	20.8	26.3	42.4	49.4
<i>Retrieval</i>	ClipOrder [109]	7.6	22.9	48.8	14.1	30.3	51.1
	VCP [19]	7.6	24.4	53.6	18.6	33.6	53.5
	GDT (ours)	25.4	51.4	75.0	57.4	73.4	88.1

Table 5: **Audio classification.** Downstream task accuracies on standard audio classification benchmarks.

Method	Top-1 Acc%	
	DCASE	ESC-50
ConvRBM [88]	-	86.5
AVTS [55]	94	82.3
DMC [46]	-	82.6
XDC [5]	93	84.8
AVID [71]	<u>96</u>	89.2
GDT (ours)	98	88.5
Human [82]	-	81.3

achieves similar state-of-the-art results to concurrent [71]. When constrained to pretraining on the AudioSet [31] dataset, we also find state-of-the-art performance among all self-supervised methods. Lastly, we show the scalability and flexibility of our GDT framework by pretraining on the IG65M dataset [32]. With this, our visual feature representation sets a new state of the art among all self-supervised methods on the UCF-101 and HMDB-51 benchmarks, particularly by a margin of > 5% on the HMDB-51 dataset. Additionally, we are the first method to beat the Kinetics supervisedly pretrained baseline using the same architecture and finetuning protocol.

Downstream audio benchmarks. For **audio classification** we find that we achieve state-of-the-art performance among all self-supervised methods on both DCASE2014 and ESC-50, and also surpass supervised performance on VGG-Sound.

5 Conclusion

We have introduced the framework of generalized data transformation which allows one to capture, in a single noise-contrastive objective, cues used in several prior contrastive and non-contrastive learning formulations, as well as easily incorporate new ones. The framework shows how new meaningful combination of transformations can be obtained, encoding valuable invariances and distinctiveness we want our representations to learn. By using the framework, we have achieved state-of-the-art results for self-supervised pretraining on standard downstream video action recognition benchmarks, even surpassing supervised pretraining. Overall, our method significantly increases the expressiveness of contrastive learning for self-supervision, making it a flexible tool for further research in the area.

Table 6: **VGG-Sound.** Downstream audio classification metrics after full-finetuning.

Method	mAP%	AUC%	d'
Supervised [17]	51.6	96.8	2.63
GDT (ours)	54.8	97.5	2.77

Broader impact

We see the research presented in this work to have a potential broader impact in three main areas over the short and long term.

Reduce bias on less curated data The promise of self-supervised methods is to learn ever more robust and general visual representation models without manual annotations. Indeed, training on ever larger datasets with ever better methods has continued to increase performance on downstream tasks and we have presented similar findings in this paper. This shows the potential and benefit of self-supervised learning compared to supervised or weakly-supervised learning, and also has the added potential to reduce the risk of incorporating biases present in the training data. As biases start in the data collection process, using less curated data and significantly more of it might be useful in having less biased models as these will be trained with more diversity. We should also note that biases present in these models might disappear once the network is fine-tuned on a target task (on which biases should, also be avoided or known). However, it is still crucial to understand this aspect in detail when it comes to deployment and we believe that research should be encouraged probing self-supervised models with regards to their underlying data distributions, in a similar way to [48, 103] for images, and as has been done more rigorously in the NLP domain for some time, e.g. [12, 80, 85, 115].

Applications in medical imaging. Using pretrained visual feature representations, such as those obtained by training on ImageNet LSVRC-12 and finetuning these on specific medical imaging tasks has been very successful [63, 90, 108]. Models obtained in such a manner outperform those trained from scratch and vice versa require less expert time for human annotation [65]. Thus far, these mostly 2D CNN models were used for transfer learning, but there are applications where the temporal dimension is key, such as heart imaging with ultra sound [47]. It is likely that self-supervised video representation models, such as the one presented in this paper will be useful for these applications, with the implications of a) increasing the accuracy of the physician’s diagnosis, b) reducing the time-cost of diagnosis, and c) facilitating remote diagnostics in places with not enough trained staff. However, a risk with algorithms in unsupervised learning is that users may put too much blind trust on the results of the algorithm (in our case a network initialization). In practice, there are no guarantees that the algorithm would find a solution fit for any particular downstream application. This needs to be carefully validated a posteriori.

Harmful content detection. The number of uploaded videos to online platforms only keeps increasing, yet automatically detecting harmful content is still in its infancy. As content is now increasingly moving towards videos, self-supervisedly trained video models may be especially useful for transfer learning. The benefits are a) the models can be more accurately detect harmful content, leading to both higher recall and precision, and b) training good classifiers requires less annotations from humans, which are in this case not just expensive but psychologically harmful.

Furthermore we encourage ways of getting the research community to participate in these developments in ways that do not require the release and distribution of such material. One recent such initiative is the hateful memes competition⁵, which although based on image understanding captures the difficulties of multi-modal learning and the nuances of understanding intention.

Acknowledgments and Disclosure of Funding

We are grateful for support from the Rhodes Trust (M.P.), Facebook (M.P.), EPSRC Centre for Doctoral Training in Autonomous Intelligent Machines & Systems [EP/L015897/1] (M.P. and Y.A.), the Open Philanthropy Project (R.F.), and the Royal Academy of Engineering under the Research Fellowship scheme (J.F.H.). We also thank Andrew Owens, Alexei Efros and Tengda Han for helpful discussions on self-supervised learning. Lastly, the authors would also like to thank Ishan Misra and Bruno Korbar from Facebook for valuable discussions and sharing insights.

⁵<https://www.drivendata.org/competitions/64/hateful-memes/>

References

- [1] <https://youtu.be/-Wr6W0Xnztk>, <https://youtu.be/-BmuSpckr3U>, 2020.
- [2] Triantafyllos Afouras, Joon Son Chung, Andrew Senior, Oriol Vinyals, and Andrew Zisserman. Deep audio-visual speech recognition. *IEEE transactions on pattern analysis and machine intelligence*, 2018.
- [3] Triantafyllos Afouras, Joon Son Chung, and Andrew Zisserman. The conversation: Deep audio-visual speech enhancement. *Interspeech*, 2018.
- [4] Triantafyllos Afouras, Joon Son Chung, and Andrew Zisserman. Deep lip reading: A comparison of models and an online application. 2018.
- [5] Humam Alwassel, Dhruv Mahajan, Lorenzo Torresani, Bernard Ghanem, and Du Tran. Self-supervised learning by cross-modal audio-video clustering. *arXiv preprint arXiv:1911.12667*, 2019.
- [6] Relja Arandjelovic and Andrew Zisserman. Look, listen and learn. In *Proc. ICCV*, 2017.
- [7] Relja Arandjelović and Andrew Zisserman. Objects that sound. In *ECCV*, 2018.
- [8] Yuki M Asano, Christian Rupprecht, and Andrea Vedaldi. Self-labelling via simultaneous clustering and representation learning. In *ICLR*, 2020.
- [9] Yusuf Aytar, Carl Vondrick, and Antonio Torralba. Soundnet: Learning sound representations from unlabeled video. In *NeurIPS*, 2016.
- [10] Philip Bachman, R Devon Hjelm, and William Buchwalter. Learning representations by maximizing mutual information across views. In *NeurIPS*, 2019.
- [11] Sagie Benaim, Ariel Ephrat, Oran Lang, Inbar Mosseri, William T. Freeman, Michael Rubinstein, Michal Irani, and Tali Dekel. Speednet: Learning the speediness in videos. In *CVPR*, 2020.
- [12] Tolga Bolukbasi, Kai-Wei Chang, James Y Zou, Venkatesh Saligrama, and Adam T Kalai. Man is to computer programmer as woman is to homemaker? debiasing word embeddings. In *NeurIPS*, 2016.
- [13] Uta Buchler, Biagio Brattoli, and Bjorn Ommer. Improving spatiotemporal self-supervision by deep reinforcement learning. In *ECCV*, 2018.
- [14] Mathilde Caron, Piotr Bojanowski, Armand Joulin, and Matthijs Douze. Deep clustering for unsupervised learning of visual features. In *ECCV*, 2018.
- [15] Mathilde Caron, Piotr Bojanowski, Julien Mairal, and Armand Joulin. Unsupervised pre-training of image features on non-curated data. In *ICCV*, 2019.
- [16] Changan Chen, Unnat Jain, Carl Schissler, Sebastia Vicenc Amengual Gari, Ziad Al-Halah, Vamsi Krishna Ithapu, Philip Robinson, and Kristen Grauman. Audio-visual embodied navigation. *arXiv preprint arXiv:1912.11474*, 2019.
- [17] Honglie Chen, Weidi Xie, Andrea Vedaldi, and Andrew Zisserman. Vggsound: A large-scale audio-visual dataset. In *ICASSP*, 2020.
- [18] Ting Chen, Simon Kornblith, Mohammad Norouzi, and Geoffrey Hinton. A simple framework for contrastive learning of visual representations. *arXiv preprint arXiv:2002.05709*, 2020.
- [19] Hyeon Cho, Taehoon Kim, Hyung Jin Chang, and Wonjun Hwang. Self-supervised spatiotemporal representation learning using variable playback speed prediction. *arXiv preprint arXiv:2003.02692*, 2020.
- [20] Joon Son Chung and Andrew Zisserman. Out of time: automated lip sync in the wild. In *Workshop on Multi-view Lip-reading, ACCV*, 2016.
- [21] Joon Son Chung, Andrew Senior, Oriol Vinyals, and Andrew Zisserman. Lip reading sentences in the wild. *CVPR*, 2017.
- [22] Virginia R. de Sa. Learning classification with unlabeled data. In *NeurIPS*, 1994.
- [23] Ali Diba, Vivek Sharma, Luc Van Gool, and Rainer Stiefelhagen. Dynamonet: Dynamic action and motion network. In *ICCV*, 2019.
- [24] Carl Doersch, Abhinav Gupta, and Alexei A Efros. Unsupervised visual representation learning by context prediction. In *ICCV*, 2015.
- [25] Jeff Donahue and Karen Simonyan. Large scale adversarial representation learning. In *Proc. ICLR*, 2019.
- [26] Basura Fernando, Hakan Bilen, Efstratios Gavves, and Stephen Gould. Self-supervised video representation learning with odd-one-out networks. In *Proc. CVPR*, 2017.

- [27] Chuang Gan, Boqing Gong, Kun Liu, Hao Su, and Leonidas J Guibas. Geometry guided convolutional neural networks for self-supervised video representation learning. In *CVPR*, 2019.
- [28] Ruohan Gao and Kristen Grauman. Co-separating sounds of visual objects. In *ICCV*, 2019.
- [29] Ruohan Gao, Rogerio Feris, and Kristen Grauman. Learning to separate object sounds by watching unlabeled video. In *ECCV*, 2018.
- [30] Ruohan Gao, Tae-Hyun Oh, Kristen Grauman, and Lorenzo Torresani. Listen to look: Action recognition by previewing audio. In *CVPR*, 2020.
- [31] Jort F. Gemmeke, Daniel P. W. Ellis, Dylan Freedman, Aren Jansen, Wade Lawrence, R. Channing Moore, Manoj Plakal, and Marvin Ritter. Audio set: An ontology and human-labeled dataset for audio events. In *ICASSP*, 2017.
- [32] Deepti Ghadiyaram, Du Tran, and Dhruv Mahajan. Large-scale weakly-supervised pre-training for video action recognition. In *CVPR*, 2019.
- [33] Spyros Gidaris, Praveer Singh, and Nikos Komodakis. Unsupervised representation learning by predicting image rotations. *ICLR*, 2018.
- [34] Spyros Gidaris, Andrei Bursuc, Nikos Komodakis, Patrick Pérez, and Matthieu Cord. Learning representations by predicting bags of visual words. In *CVPR*, 2020.
- [35] Priya Goyal, Piotr Dollár, Ross Girshick, Pieter Noordhuis, Lukasz Wesolowski, Aapo Kyrola, Andrew Tulloch, Yangqing Jia, and Kaiming He. Accurate, large minibatch SGD: training imagenet in 1 hour. *arXiv preprint arXiv:1706.02677*, 2017.
- [36] Michael Gutmann and Aapo Hyvärinen. Noise-contrastive estimation: A new estimation principle for unnormalized statistical models. In *AISTATS*, 2010.
- [37] Raia Hadsell, Sumit Chopra, and Yann LeCun. Dimensionality reduction by learning an invariant mapping. In *CVPR*, 2006.
- [38] Tengda Han, Weidi Xie, and Andrew Zisserman. Video representation learning by dense predictive coding. In *ICCV Workshops*, 2019.
- [39] David Harwath, Adria Recasens, Dídac Surís, Galen Chuang, Antonio Torralba, and James Glass. Jointly discovering visual objects and spoken words from raw sensory input. In *ECCV*, 2018.
- [40] Kaiming He, Xiangyu Zhang, Shaoqing Ren, and Jian Sun. Deep residual learning for image recognition. In *CVPR*, 2016.
- [41] Kaiming He, Haoqi Fan, Yuxin Wu, Saining Xie, and Ross Girshick. Momentum contrast for unsupervised visual representation learning, 2019.
- [42] Olivier J Hénaff, Ali Razavi, Carl Doersch, SM Eslami, and Aaron van den Oord. Data-efficient image recognition with contrastive predictive coding. *arXiv preprint arXiv:1905.09272*, 2019.
- [43] Geoffrey E Hinton and Ruslan R Salakhutdinov. Reducing the dimensionality of data with neural networks. *Science*, 2006.
- [44] Geoffrey E Hinton, Simon Osindero, and Yee-Whye Teh. A fast learning algorithm for deep belief nets. *Neural computation*, 2006.
- [45] R Devon Hjelm, Alex Fedorov, Samuel Lavoie-Marchildon, Karan Grewal, Phil Bachman, Adam Trischler, and Yoshua Bengio. Learning deep representations by mutual information estimation and maximization. In *ICLR*, 2019.
- [46] Di Hu, Feiping Nie, and Xuelong Li. Deep multimodal clustering for unsupervised audiovisual learning. In *CVPR*, 2019.
- [47] Weilin Huang, Christopher P Bridge, J Alison Noble, and Andrew Zisserman. Temporal heartnet: towards human-level automatic analysis of fetal cardiac screening video. In *MICCAI*, 2017.
- [48] Ali Jahanian*, Lucy Chai*, and Phillip Isola. On the "steerability" of generative adversarial networks. In *ICLR*, 2020.
- [49] Longlong Jing and Yingli Tian. Self-supervised spatiotemporal feature learning by video geometric transformations. *arXiv preprint arXiv:1811.11387*, 2018.
- [50] Will Kay, Joao Carreira, Karen Simonyan, Brian Zhang, Chloe Hillier, Sudheendra Vijayanarasimhan, Fabio Viola, Tim Green, Trevor Back, Paul Natsev, et al. The kinetics human action video dataset. *arXiv preprint arXiv:1705.06950*, 2017.
- [51] Evangelos Kazakos, Arsha Nagrani, Andrew Zisserman, and Dima Damen. Epic-fusion: Audio-visual temporal binding for egocentric action recognition. In *ICCV*, 2019.

- [52] Prannay Khosla, Piotr Teterwak, Chen Wang, Aaron Sarna, Yonglong Tian, Phillip Isola, Aaron Maschinot, Ce Liu, and Dilip Krishnan. Supervised contrastive learning. *arXiv preprint arXiv:2004.11362*, 2020.
- [53] Dahun Kim, Donghyeon Cho, and In So Kweon. Self-supervised video representation learning with space-time cubic puzzles. In *AAAI*, 2019.
- [54] Diederik P. Kingma and Jimmy Ba. Adam: A method for stochastic optimization. In *ICLR*, 2015.
- [55] Bruno Korbar, Du Tran, and Lorenzo Torresani. Cooperative learning of audio and video models from self-supervised synchronization. In *NeurIPS*, 2018.
- [56] Bruno Korbar, Du Tran, and Lorenzo Torresani. Scsampler: Sampling salient clips from video for efficient action recognition. In *ICCV*, 2019.
- [57] Hildegard Kuehne, Hueihan Jhuang, Estíbaliz Garrote, Tomaso Poggio, and Thomas Serre. HMDB: a large video database for human motion recognition. In *ICCV*, 2011.
- [58] Quoc V Le, Will Y Zou, Serena Y Yeung, and Andrew Y Ng. Learning hierarchical invariant spatio-temporal features for action recognition with independent subspace analysis. In *CVPR*, 2011.
- [59] Honglak Lee, Alexis Battle, Rajat Raina, and Andrew Y Ng. Efficient sparse coding algorithms. In *NeurIPS*, 2007.
- [60] Hsin-Ying Lee, Jia-Bin Huang, Maneesh Singh, and Ming-Hsuan Yang. Unsupervised representation learning by sorting sequences. In *ICCV*, 2017.
- [61] Junnan Li, Pan Zhou, Caiming Xiong, Richard Socher, and Steven CH Hoi. Prototypical contrastive learning of unsupervised representations. *arXiv preprint arXiv:2005.04966*, 2020.
- [62] Tianhao Li and Limin Wang. Learning spatiotemporal features via video and text pair discrimination. *arXiv preprint arXiv:2001.05691*, 2020.
- [63] Geert Litjens, Thijs Kooi, Babak Ehteshami Bejnordi, Arnaud Arindra Adiyoso Setio, Francesco Ciompi, Mohsen Ghafoorian, Jeroen Awm Van Der Laak, Bram Van Ginneken, and Clara I Sánchez. A survey on deep learning in medical image analysis. *Medical image analysis*, 2017.
- [64] Yang Liu, Samuel Albanie, Arsha Nagrani, and Andrew Zisserman. Use what you have: Video retrieval using representations from collaborative experts. In *BMVC*, 2019.
- [65] Alexander Selvikvåg Lundervold and Arvid Lundervold. An overview of deep learning in medical imaging focusing on mri. *Zeitschrift für Medizinische Physik*, 2019. Special Issue: Deep Learning in Medical Physics.
- [66] Dezhao Luo, Chang Liu, Yu Zhou, Dongbao Yang, Can Ma, Qixiang Ye, and Weiping Wang. Video cloze procedure for self-supervised spatio-temporal learning. In *AAAI*, 2020.
- [67] Zelun Luo, Boya Peng, De-An Huang, Alexandre Alahi, and Li Fei-Fei. Unsupervised learning of long-term motion dynamics for videos. In *CVPR*, 2017.
- [68] Antoine Miech, Jean-Baptiste Alayrac, Lucas Smaira, Ivan Laptev, Josef Sivic, and Andrew Zisserman. End-to-end learning of visual representations from uncurated instructional videos. In *CVPR*, 2020.
- [69] Ishan Misra and Laurens van der Maaten. Self-supervised learning of pretext-invariant representations. In *CVPR*, 2020.
- [70] Ishan Misra, C Lawrence Zitnick, and Martial Hebert. Shuffle and learn: unsupervised learning using temporal order verification. In *ECCV*, 2016.
- [71] Pedro Morgado, Nuno Vasconcelos, and Ishan Misra. Audio-visual instance discrimination with cross-modal agreement. *arXiv preprint arXiv:2004.12943*, 2020.
- [72] Arsha Nagrani, Chen Sun, David Ross, Rahul Sukthankar, Cordelia Schmid, and Andrew Zisserman. Speech2action: Cross-modal supervision for action recognition. In *CVPR*, 2020.
- [73] Jiquan Ngiam, Aditya Khosla, Mingyu Kim, Juhan Nam, Honglak Lee, and Andrew Y Ng. Multimodal deep learning. In *ICML*, 2011.
- [74] Mehdi Noroozi and Paolo Favaro. Unsupervised learning of visual representations by solving jigsaw puzzles. In *ECCV*, 2016.
- [75] Mehdi Noroozi, Hamed Pirsiavash, and Paolo Favaro. Representation learning by learning to count. In *ICCV*, 2017.
- [76] Aaron van den Oord, Yazhe Li, and Oriol Vinyals. Representation learning with contrastive predictive coding. *arXiv preprint arXiv:1807.03748*, 2018.
- [77] Andrew Owens and Alexei A Efros. Audio-visual scene analysis with self-supervised multi-sensory features. In *ECCV*, 2018.

- [78] Andrew Owens, Jiajun Wu, Josh H McDermott, William T Freeman, and Antonio Torralba. Ambient sound provides supervision for visual learning. In *ECCV*, 2016.
- [79] Daniel S. Park, William Chan, Yu Zhang, Chung-Cheng Chiu, Barret Zoph, Ekin D. Cubuk, and Quoc V. Le. SpecAugment: A simple data augmentation method for automatic speech recognition. In *INTERSPEECH*, 2019.
- [80] Ji Ho Park, Jamin Shin, and Pascale Fung. Reducing gender bias in abusive language detection. In *EMNLP*, 2018.
- [81] Deepak Pathak, Philipp Krahenbuhl, Jeff Donahue, Trevor Darrell, and Alexei A Efros. Context encoders: Feature learning by inpainting. In *CVPR*, 2016.
- [82] Karol J. Piczak. Esc: Dataset for environmental sound classification. In *ACM Multimedia*, 2015.
- [83] AJ Piergiovanni, Anelia Angelova, and Michael S. Ryoo. Evolving losses for unsupervised video representation learning. In *CVPR*, 2020.
- [84] Gerasimos Potamianos, Chalapathy Neti, Guillaume Gravier, Ashutosh Garg, and Andrew W Senior. Recent advances in the automatic recognition of audiovisual speech. *Proceedings of the IEEE*, 91(9):1306–1326, 2003.
- [85] Yusu Qian, Urwa Muaz, Ben Zhang, and Jae Won Hyun. Reducing gender bias in word-level language models with a gender-equalizing loss function. In *ACL: Student Research Workshop*, 2019.
- [86] Marc' aurelio Ranzato, Fu Jie Huang, Y-Lan Boureau, and Yann LeCun. Unsupervised learning of invariant feature hierarchies with applications to object recognition. In *CVPR*, 2007.
- [87] Andrew Rouditchenko, Hang Zhao, Chuang Gan, Josh McDermott, and Antonio Torralba. Self-supervised audio-visual co-segmentation. In *ICASSP*, 2019.
- [88] Hardik B. Sailor, Dharmesh M Agrawal, and Hemant A Patil. Unsupervised filterbank learning using convolutional restricted boltzmann machine for environmental sound classification. In *INTERSPEECH*, 2017.
- [89] Nawid Sayed, Biagio Brattoli, and Björn Ommer. Cross and learn: Cross-modal self-supervision. *German Conference on Pattern Recognition*, 2018.
- [90] Thomas Schlegl, Joachim Ofner, and Georg Langs. Unsupervised pre-training across image domains improves lung tissue classification. In *MICCAI: Medical Computer Vision Workshop*, 2014.
- [91] Arda Senocak, Tae-Hyun Oh, Junsik Kim, Ming-Hsuan Yang, and In So Kweon. Learning to localize sound source in visual scenes. In *CVPR*, 2018.
- [92] Karen Simonyan and Andrew Zisserman. Two-stream convolutional networks for action recognition in videos. In *ICLR*, 2014.
- [93] Kihyuk Sohn. Improved deep metric learning with multi-class n-pair loss objective. In *NeurIPS*, 2016.
- [94] Khurram Soomro, Amir Roshan Zamir, and Mubarak Shah. UCF101: A dataset of 101 human actions classes from videos in the wild. *arXiv preprint arXiv:1212.0402*, 2012.
- [95] D. Stowell, D. Giannoulis, E. Benetos, M. Lagrange, and M. D. Plumbley. Detection and classification of acoustic scenes and events. *IEEE Transactions on Multimedia*, 2015.
- [96] Chen Sun, Fabien Baradel, Kevin Murphy, and Cordelia Schmid. Contrastive bidirectional transformer for temporal representation learning. *arXiv preprint arXiv:1906.05743*, 2019.
- [97] Chen Sun, Austin Myers, Carl Vondrick, Kevin Murphy, and Cordelia Schmid. Videobert: A joint model for video and language representation learning. In *ICCV*, 2019.
- [98] Yonglong Tian, Dilip Krishnan, and Phillip Isola. Contrastive multiview coding. *arXiv preprint arXiv:1906.05849*, 2019.
- [99] Yonglong Tian, Chen Sun, Ben Poole, Dilip Krishnan, Cordelia Schmid, and Phillip Isola. What makes for good views for contrastive learning. *arXiv preprint arXiv:2005.10243*, 2020.
- [100] Du Tran, Heng Wang, Lorenzo Torresani, Jamie Ray, Yann LeCun, and Manohar Paluri. A closer look at spatiotemporal convolutions for action recognition. In *CVPR*, 2018.
- [101] Du Tran, Heng Wang, Lorenzo Torresani, Jamie Ray, Yann LeCun, and Manohar Paluri. A closer look at spatiotemporal convolutions for action recognition. In *CVPR*, 2018.
- [102] Carl Vondrick, Hamed Pirsiavash, and Antonio Torralba. Generating videos with scene dynamics. In *NeurIPS*, 2016.
- [103] Andrey Voynov and Artem Babenko. Unsupervised discovery of interpretable directions in the gan latent space. *arXiv preprint arXiv:2002.03754*, 2020.

- [104] Jiangliu Wang, Jianbo Jiao, Linchao Bao, Shengfeng He, Yunhui Liu, and Wei Liu. Self-supervised spatio-temporal representation learning for videos by predicting motion and appearance statistics. In *CVPR*, 2019.
- [105] Donglai Wei, Joseph J Lim, Andrew Zisserman, and William T Freeman. Learning and using the arrow of time. In *CVPR*, 2018.
- [106] Zhirong Wu, Yuanjun Xiong, Stella X. Yu, and Dahua Lin. Unsupervised feature learning via non-parametric instance discrimination. In *CVPR*, 2018.
- [107] Fanyi Xiao, Yong Jae Lee, Kristen Grauman, Jitendra Malik, and Christoph Feichtenhofer. Audiovisual slowfast networks for video recognition. *arXiv preprint arXiv:2001.08740*, 2020.
- [108] Yiting Xie and David Richmond. Pre-training on grayscale imagenet improves medical image classification. In *ECCV*, 2018.
- [109] Dejing Xu, Jun Xiao, Zhou Zhao, Jian Shao, Di Xie, and Yueting Zhuang. Self-supervised spatiotemporal learning via video clip order prediction. In *CVPR*, 2019.
- [110] Richard Zhang, Phillip Isola, and Alexei A. Efros. Colorful image colorization. In *Proc. ECCV*, 2016.
- [111] Richard Zhang, Phillip Isola, and Alexei A Efros. Split-brain autoencoders: Unsupervised learning by cross-channel prediction. In *CVPR*, 2017.
- [112] Xiangyu Zhang, Xinyu Zhou, Mengxiao Lin, and Jian Sun. Shufflenet: An extremely efficient convolutional neural network for mobile devices. In *CVPR*, 2018.
- [113] Hang Zhao, Chuang Gan, Andrew Rouditchenko, Carl Vondrick, Josh McDermott, and Antonio Torralba. The sound of pixels. In *ECCV*, 2018.
- [114] Hang Zhao, Chuang Gan, Wei-Chiu Ma, and Antonio Torralba. The sound of motions. In *ICCV*, 2019.
- [115] Jieyu Zhao, Tianlu Wang, Mark Yatskar, Ryan Cotterell, Vicente Ordonez, and Kai-Wei Chang. Gender bias in contextualized word embeddings. In *Proceedings of the 2019 Conference of the North American Chapter of the Association for Computational Linguistics: Human Language Technologies, Volume 1 (Long and Short Papers)*, pages 629–634, 2019.

A Appendix

A.1 Theory

Full knowledge of the contrast function c only specifies the level sets of the representation f .

Lemma 1. *The contrast $c(x_1, x_2) = \delta_{f(x_1)=f(x_2)}$ defines $f = \iota \circ \hat{f}$ up to an injection $\iota : \mathcal{X}/f \rightarrow \mathcal{Y}$, where \mathcal{X}/f is the quotient space and $\hat{f} : \mathcal{X} \rightarrow \mathcal{X}/f$ is the projection on the quotient.*

Proof. This is a well known fact in elementary algebra. Recall that the quotient \mathcal{X}/f is just the collection of subsets $X \subset \mathcal{X}$ where $f(x)$ is constant. It is easy to see that this is a partition of \mathcal{X} . Hence, we can define the map $\hat{f} : X \mapsto f(x)$ where x is any element of X (this is consistent since $f(x)$ has, by definition, only one value over X). Furthermore, if $\iota : x \mapsto X = \{x \in \mathcal{X} : f(x') = f(x)\}$ is the projection of x to its equivalence class X , we have $f(x) = \hat{f}(\iota(x))$. \square

Lemma 2. *$c(x_1, x_2) = 1$ is an equivalence relation if, and only if, there exists a function f such that $c(x_1, x_2) = \delta_{f(x_1)=f(x_2)}$.*

Proof. If $c(x_1, x_2) = 1$ defines an equivalence relation on \mathcal{X} , then such a function is given by the projection on the quotient $\hat{f} : \mathcal{X} \rightarrow \mathcal{X}/c = \mathcal{Y}$. On the other hand, setting $c(x_1, x_2) = \delta_{f(x_1)=f(x_2)} = 1$ for any given function f is obviously reflexive, symmetric and transitive because the equality $f(x_1) = f(x_2)$ is. \square

The following lemma suggests that defining a contrast $c(T, T')$ on transformations instead of data samples is usually acceptable.

Lemma 3. *If $c(T, T') = 1$ defines an equivalence relation on GDTs, and if $TD = TD' \Rightarrow T = T'$ (i.e. different transformations output different samples), then setting $c(TD, T'D) = c(T, T')$ defines part of an admissible sample contrast function.*

Proof. If $x = TD$, $x' = T'D$ are obtained from some transformations T and T' , then these must be unique by assumption. Thus, setting $c(x, x') = c(T, T')$ is well posed. Reflectivity, symmetry and transitivity are then inherited from the latter. \square

Lemma 4. *Let $c(t_m, t'_m) = 1$ be reflexive, symmetric and transitive. Their product $c(T, T') = \prod_{m=1}^M c(t_m, t'_m) = 1$ has then the same properties.*

Proof. The reflexive and symmetric properties are obviously inherited. For the transitive property, note that $c(T, T') = 1$ if, and only if, $\forall m : c(t_m, t'_m) = 1$. Then consider:

$$\begin{aligned} c(T, T') = c(T', T'') = 1 &\Rightarrow \forall m : c(t_m, t'_m) = c(t'_m, t''_m) = 1 \\ &\Rightarrow \forall m : c(t_m, t''_m) = 1 \Rightarrow c(T, T'') = 1. \end{aligned}$$

\square

A.2 Generality of GDT

Here, we show that our GDT formulation can encapsulate and unify other self-supervised works in the literature. We break it down it to two sections:

Mapping contrastive to GDT contrastive Recently, a number of papers have presented contrastive formulations for image representation learning such as, NPID [106], PIRL [69], MoCo [41] and SimCLR [98]. These methods are all essentially built on we have introduced as the “data-sampling transformation” $\mathcal{T} = (i, g)$, that samples an image with index i and applies augmentation g . For NPID, MoCo and SimCLR, the main objective is to solely be distinctive to the image index, hence $K = K_i K_g = 1$ for NPID, due to the use of a memorybank and $K = K_i K_g = 2$ for SimCLR and MoCo. For PIRL, one additional transformation to be invariant to is added. For example for PIRL with rotation, the data-sampling variance loss is only applied to the non-rotated inputs $K = K_i K_g = 1$ to the memorybank, while the rotated examples are used for constructing an invariance loss to the original ones, such that $K_g = 2$.

Non-contrastive to contrastive reduction In non-contrastive self-supervised formulations, one trains $\Phi(x) = y$ to regress y from x , where y is some “pretext” task label. These labels can be obtained from the data, e.g. arrow of time [105], rotation [33, 49], shuffled frames [70], jigsaw configurations [53, 75], playback speed [11, 19]. Equivalent tasks can thus be constructed in our GDT formulation by introducing transformations such as reversal of time or spatial rotation, and using it as a negative example, i.e. being distinctive to this transformation. For example, for rotations, clips rotated by the same amount would be considered as positive pairs, while any other rotation would be used to construct the set of negative pairs. Thus pretext task-originating transformations that have not even been explored yet can be put into our framework and, as we show in this paper, be naturally combined with other transformations leading to even stronger representations.

A.3 Modality ablation

Table A.1: **Multi-modal learning**, m_m .

Modalities	HMDB		UCF	
Epochs	50	100	50	100
Within-modal	29.1	32.9	68.3	72.2
Cross-modal	<u>55.1</u>	<u>56.9</u>	<u>85.1</u>	<u>87.9</u>

A.4 Pretraining details

For NCE contrastive learning, the temperature ρ is set as $1/0.07$. For optimizing these networks, we use SGD. The SGD weight decay is 10^{-5} and the SGD momentum is 0.9. We use a mini-batch size of 12 on each of our 64 GPUs giving an effective batch size of 768 for distributed training. The initial learning rate is set to 0.01 which we linearly scale with the number of GPUs, after following a gradual warm-up schedule for the first 10 epochs [35]. We train for 200 epochs overall except in our ablations, where we train for 100 epochs.

A.5 Ablation experiment details

For the ablations, we only train for 100 epochs unless specified otherwise. For both downstream tasks, we only evaluate on the first fold each but found the performance between folds to be close (within 1-2%).

A.6 Full video action retrieval table

In Table A.2 we show the full table on video action retrieval and compare to several of our models, pretrained on different datasets.

Table A.2: **Full retrieval table.**

Recall @	HMDB					UCF				
	1	5	10	20	50	1	5	10	20	50
Supervised (Kinetics)	49.1	74.4	83.9	90.6	96.4	86.9	94.6	96.5	98.1	99.0
ST-Puzzle [53]	-	-	-	-	-	19.7	28.5	33.5	40.0	49.4
OPN [60]	-	-	-	-	-	19.9	28.7	34.0	40.6	51.6
ST Order [13]	-	-	-	-	-	25.7	36.2	42.2	49.2	59.5
ClipOrder [109]	7.6	22.9	34.4	48.8	68.9	14.1	30.3	40.4	51.1	66.5
SpeedNet [11]	-	-	-	-	-	13.0	28.1	37.5	49.5	65.0
VCP [66]	7.6	24.4	36.3	53.6	76.4	18.6	33.6	42.5	53.5	68.1
VSP [19]	10.3	26.6	38.8	54.6	76.8	24.6	41.9	51.3	62.7	76.9
GDT (Kinetics)	25.4	51.4	63.9	75.0	87.8	57.4	73.4	80.8	88.1	92.9
GDT (VGG-Sound)	28.4	55.1	67.2	79.3	91.1	63.4	79.6	85.0	90.1	95.2
GDT (Audioset)	30.6	58.0	69.8	79.9	91.0	65.9	82.6	88.2	92.2	96.6
GDT (IG65M)	36.1	61.1	70.8	79.7	92.1	75.7	87.2	90.7	93.5	96.6

A.7 Full video action recognition table

Table A.3: **State-of-the-art on video action recognition.** Self-supervised and fully-supervised trained methods on UCF101 and HMDB51 benchmarks. We follow the standard protocol and report the average top-1 accuracy over the official splits and show results for finetuning the whole network. Note that we find the supervised baseline to be around 6% and 2% better than reported in [5]. Methods with [†] indicate the additional use of video titles as supervision. Methods with * use ASR generated text.

Method	Architecture	Pretrain Dataset	Top-1 Acc%	
			HMDB	UCF
Full supervision	R(2+1)D-18	ImageNet	46.7	82.8
Full supervision [5]	R(2+1)D-18	Kinetics-400	63.6	93.1
Full supervision (ours)	R(2+1)D-18	Kinetics-400	70.4	95.0
Full supervision [101]	R(2+1)D-34	Kinetics-400	74.5	96.8
<i>Using UCF</i>				
Shuffle and Learn [70]	CaffeNet	UCF	18.1	50.2
VGAN [102]	VGAN	Flickr	-	52.1
LT-Motion [67]	VGG-16	UCF	-	53.0
Geometry [27]	CaffeNet	UCF	23.3	55.1
OPN [60]	VGG	UCF	23.8	56.3
ST Order [13]	CaffeNet	UCF	25.0	58.6
CMC [98]	CaffeNet	UCF	26.7	59.1
VCP [66]	R(2+1)D-18	UCF	32.2	66.3
Cross and Learn [89]	VGG-16	UCF	33.0	70.5
<i>Using Kinetics</i>				
ClipOrder [109]	R(2+1)D-18	Kinetics-400	30.9	72.4
MotionPred [104]	C3D	Kinetics-400	33.4	61.2
RotNet3D [49]	3D-ResNet18	Kinetics-600	33.7	62.9
ST-Puzzle [53]	3D-ResNet18	Kinetics-400	33.7	65.8
DPC [38]	3D-ResNet34	Kinetics-400	35.7	75.7
VPS [19]	R3D	Kinetics-400	36.8	74.8
SpeedNet [11]	I3D	Kinetics-400	43.7	66.7
AoT [105]	T-CAM	Kinetics-400	-	79.4
CBT [96]	S3D	Kinetics-600	44.6	79.5
Multisensory [77]	3D-ResNet18	Kinetics-400	-	82.1
XDC [5]	R(2+1)D-18	Kinetics-400	47.1	84.2
AV Sync+RotNet [107]	AVSlowFast	Kinetics-400	54.6	87.0
AVTS [55]	MC3-18	Kinetics-400	56.9	85.8
CPD [62] ^{†*}	3D-Resnet50	Kinetics-400	57.7	88.7
AVID [71]	R(2+1)D-18	Kinetics-400	60.8	87.5
GDT (ours)	R(2+1)D-18	Kinetics-400	60.0	89.3
<i>Using other datasets</i>				
L ³ -Net [6]	VGG-16	AudioSet	40.2	72.3
Speech2Action* [72]	S3D-G	MovieDataset	58.1	-
DynamoNet [23]	ResNext101	Youtube8M	58.6	87.3
XDC [5]	R(2+1)D-18	AudioSet	61.0	91.2
MIL-NCE [68]*	S3D	HowTo100M	61.0	91.3
AVTS [55]	MC3-18	AudioSet	61.6	89.0
AVID [71]	R(2+1)D-18	AudioSet	64.7	91.5
ELo [83]	R(2+1)D-50x3	Youtube-2M	67.4	93.8
XDC [5]	R(2+1)D-18	IG65M	67.4	94.2
GDT (ours)	R(2+1)D-18	VGGSound (170K)	61.9	89.4
GDT (ours)	R(2+1)D-18	AudioSet (1.7M)	66.1	92.5
GDT (ours)	R(2+1)D-18	IG65M	72.8	95.2

A.8 Evaluation details

Video During training, we take 10 random clips of length 32 frames from each video. For video clip augmentations, we follow a standard protocol as in [55]. During evaluation, we uniformly sample 10 clips from each video, average softmax scores, and predict the class having the highest mean softmax score. We then measure the mean video top-1 accuracy across all videos and all official folds. We use SGD with initial learning rate 0.0025, which we gradually warm up to $2 \cdot 10^{-2}$ in the first 2 epochs. The weight decay is set to $5 \cdot 10^{-3}$ and momentum to 0.9. We use a mini-batch size of 32 and train for 12 epochs with the learning rate multiplied by $5 \cdot 10^{-2}$ at 6 and 10 epochs. We compare our GDT pretrained model with both self-supervised methods, and supervised pretraining, and report average top-1 accuracies on UCF101 and HMDB-51 action recognition task across three folds in table A.3.

Few-shot classification We follow the protocol in [49] and evaluate our our GDT pretrained network using few-shot classification on the UCF-101 dataset, and additionally on HMDB-51. We randomly sample n videos per class from the train set, average the encoder’s global average pooling features from ten clips per training sample and measure classification performance on the validation set after training a SVM with ‘one-vs-all’ and $C = 1$.

Retrieval We follow the standard protocol as outlined in [109]. We use the split 1 of UCF101, and additionally HMDB-51. We uniformly sample 10 clips per video, and average the max-pooled features after the last residual block for each clip per video. We use these averaged features from the validation set to query the videos in the training set. The cosine distance of representations between the query clip and all clips in the training set are computed. When the class of a test clip appears in the classes of k nearest training clips, it is considered to be correctly predicted. We report accuracies for $k = 1, 5, 10, 20, 50$ and compare with the other self-supervised methods on UCF101 and HMDB-51 in table A.2.

Audio We extract 10 equally spaced 2-second sub-clips from each full audio sample of ESC-50 [82] and 60 1-second sub-clips from each full sample of DCASE2014 [95]. ESC-50 is an environmental sound classification dataset which has 2K clips of 50 different audio classes. DCASE2014 is an acoustic scenes and event classification dataset which has 100 training clips of 10 different audio classes. We save the activations that result from the audio encoder to quickly train the linear classifiers. We use activations after the last convolutional layer of the ResNet-18 and apply a max pooling with kernel size (1,3) and stride of (1,2) without padding to the output. For both datasets, we then optimize a L2 regularized linear layer with batch size 512 using the Adam optimizer [54] with learning rate $1 \cdot 10^{-4}$, weight-decay set to $5 \cdot 10^{-4}$ and the default parameters. The classification score for each audio sample is computed by averaging the sub-clip scores in the sample, and then predicting the class with the highest score. The mean top-1 accuracy is then taken across all audio clips and averaged across all official folds. For VGG-Sound [17], we follow their evaluation metrics but follow a much shorter training schedule as our model is pretrained. We optimize the network with batch size 128 using the Adam optimizer [54] with learning rate $1 \cdot 10^{-4}$ for the pretrained backbone and $1 \cdot 10^{-3}$ for the newly randomly initialized linear layer, weight-decay set to $1 \cdot 10^{-5}$ and the default parameters. We drop the learning rate once at 10 epochs and train for 30 epochs, which takes less than 10h on a single Nvidia GTX 1080 Titan GPU.